A Droplet-Based Signal Reconstruction Approach to Channel Modeling in Molecular Communication

Fatih Gulec and Baris Atakan

***Abstract*—In this article, a novel droplet-based signal reconstruction (SR) approach to channel modeling, which considers liquid droplets as information carriers instead of molecules in the molecular communication (MC) channel, is proposed for practical sprayer-based macroscale MC systems. These practical MC systems are significant, since they can be used in order to investigate airborne pathogen transmission with biological sensors due to the similar mechanisms of sneezing/coughing and sprayer. Our proposed approach takes a two-phase flow which is generated by the interaction of droplets in liquid phase with air molecules in gas phase into account. Two-phase flow is combined with the SR of the receiver (RX) to propose a channel model. The SR part of the model quantifies how the accuracy of the sensed molecular signal in its reception volume depends on the sensitivity response of the RX and the adhesion/detachment process of droplets. The proposed channel model is validated by employing experimental data.**

***Index Terms*—Macroscale molecular communication, channel modeling, practical models, signal reconstruction, airborne pathogen transmission.**

I. Introduction

MOLECULAR communication (MC) is a prominent communication paradigm which can pave the way for potential macroscale applications. The experimental pioneering study given in [1] shows that a MC link between an alcohol sprayer as the transmitter (TX) and an alcohol sensor as the receiver (RX) can be accomplished. This study is improved via multiple input multiple output (MIMO) technique in [2]. Reference [3] proposes a platform using the pH level of chemicals to encode information symbols where this method is further investigated in a macroscale fluidic platform in [4]. In [5], a platform which employs magnetic nanoparticles as information carrier molecules is proposed. Reference [6] introduces an odor generator and a mass spectrometer as the TX and RX for macroscale MC, respectively. In [7], planar laser induced fluorescence (PLIF) method is employed for a macroscale MC testbed.

In a macroscale MC application, employing an accurate channel model enables a more efficient information transfer between the TX and RX. In addition, the location of a molecular TX can be estimated via accurate channel models [8]–[10]. As an exemplary application, an infected human emitting pathogen-laden droplets into the air through sneezing or coughing can be considered as a molecular TX in public places. By deploying biological sensors as molecular RXs, this scenario can be evaluated as a macroscale MC system [11]. Actually, the communication between a sneezing/coughing human and a biological sensor is very similar to the system given in [1] and used in our study, since sneezing/coughing can be considered as spraying droplets into the air with an initial velocity. Therefore, an accurate channel model in such a practical setup can be employed to model the spreading mechanism of infectious diseases through airborne transmission and detecting diseases in public places. In [12] and [13], channel models for the platform in [1] are derived by modifying the solution of the diffusion equation and model coefficients are estimated by fitting experimental data. Since the models in [12] and [13] are based on the molecule diffusion assumption, correction factors are needed to modify the diffusion equation. In these studies, it is not clearly known what fitted parameters of the modified diffusion equation are physically related to. Since the TX sprays liquid droplets rather than molecules and droplets are larger with respect to molecules, only diffusion is not sufficient for channel modeling in practical scenarios. Thus, initial velocities and interactions of droplets with air molecules and the surface of the sensor (RX) need to be considered. Hence, a fluid dynamics perspective considering droplets as information carriers is required for a more accurate channel model. In [14] and [15], turbulent flows and vortex rings without considering droplets are used with this perspective. However, the accuracy of the received signals by the sensor is not considered. Therefore, the droplet-sensor interaction and the accuracy of the sensed concentration by the sensor need to be taken into account.

In contrast to the models in [12] and [13] based on the diffusion of molecules, this article proposes a more realistic system model which reveals the physical meanings of the channel parameters. In this approach, droplets sprayed by the TX are considered as information carriers in the channel rather than diffusing molecules. The interaction of these droplets with air generates a two-phase flow where the first phase is liquid and the second phase is gas. In two-phase flow, droplets and air molecules move together in liquid and gas phases, respectively. The TX is modeled as a directed emitter with a predefined beamwidth. Droplets are assumed to move in a cone shaped volume determined by this beamwidth. The model also quantifies how accurate the transmitted signal is reconstructed by the RX by examining movements of droplets, interactions among droplets and surface of the sensor. Therefore, this part of the

Manuscript received March 6, 2020; revised August 11, 2020 and October 10, 2020; accepted November 28, 2020. Date of publication December 9, 2020; date of current version March 29, 2021. This work was supported by the Scientific and Technological Research Council of Turkey (TUBITAK) under Grant 119E041. The associate editor coordinating the review of this article and approving it for publication was W. Guo. *(Corresponding author: Fatih Gulec.)*

The authors are with the Department of Electrical and Electronics Engineering, Izmir Institute of Technology, 35430 Izmir, Turkey (e-mail: fatihgulec@iyte.edu.tr; barisatakan@iyte.edu.tr).

Digital Object Identifier 10.1109/TMBMC.2020.3043484

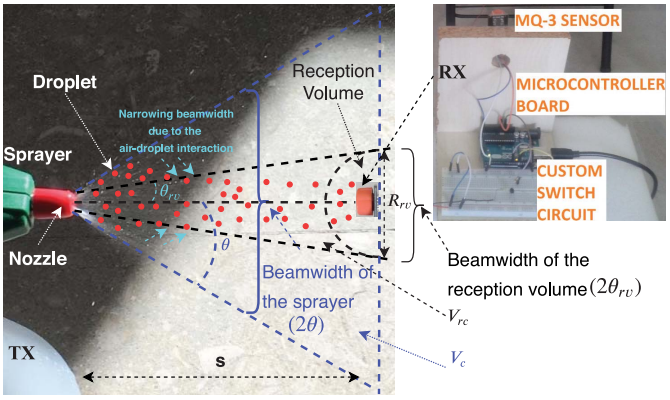

Fig. 1. The experimental setup and parameters.

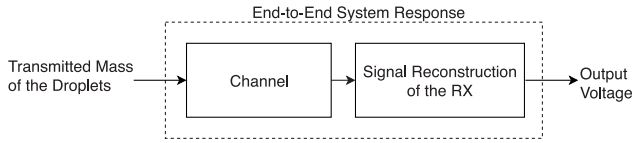

Fig. 2. Block diagram of the end-to-end system model.

model is called as signal reconstruction (SR). The SR involves two consecutive processes which are the adhesion/detachment process of droplets and the sensitivity response of the sensor. The resulting end-to-end system response is derived and validated by experimental data. It is revealed that the end-to-end system response of a practical MC system depends on the distance, parameters of the sensor measurement circuit, sensitivity characteristic of the sensor, beamwidth of the TX, spray coefficient and reaction rate constants in the adhesion/detachment process.

II. A Practical Channel Model Based on Fluid Dynamics and Signal Reconstruction

In this section, we explain our experimental setup and introduce the end-to-end system model.

A. Experimental Setup

In the experimental setup given in Fig. 1, the TX is an electric sprayer which emits ethanol droplets and the RX is an MQ-3 alcohol sensor. The TX and RX are controlled via an Arduino Uno microcontroller board by the help of a switch circuit. The TX sprays droplets with an initial velocity during the emission time (T_e). In contrast to experimental setups in [12] and [13], no fan is employed to drift droplets towards the RX. The TX and RX are aligned on the horizontal axis.

B. End-to-End System Model

For the system model shown in Fig. 2, the transmitted mass of droplets is taken as the input and the measured sensor voltage is the output of the system. The end-to-end system impulse response ($E_{out}(t)$) is defined as the system's output to a short spray emission along T_e (without a fan) which can be considered as an impulsive input signal. For the derivation of $E_{out}(t)$, the propagation time of droplets (t_0) is needed to be estimated. However, we only focus on the signal after t_0. Solely, the effect of two-phase flow on the signal in the reception volume (RV) of the RX is investigated. In addition, the initial offset voltage of the sensor is eliminated by subtracting the sensor voltage at t_0 from the whole signal.

1) The Effect of Two-Phase Flow on the Initial Concentration in the Reception Volume: As shown in Fig. 1, droplets are assumed to move in a cone-shaped volume [16] and the beamwidth (2θ) is defined as the initial spraying angle of the sprayer's nozzle. The interaction among droplets and air molecules creates a two-phase flow where droplets and air molecules move together as a mixture [17]. Here, the first phase is the liquid phase of droplets and the second phase is the gas phase of air molecules. Due to this interaction, the majority of droplets move in a narrower beamwidth, as they propagate in the channel [16]. This narrower beamwidth, denoted by $2\theta_{rv}$, is assumed to encompass the RV as illustrated in Fig. 1. Hence, the beam of droplets forms two concentric cones. The volume and base diameter of the inner cone are denoted by V_{rc} and R_{rv}, respectively. The volume of the outer cone is V_c and the distance between the TX and RX is s as depicted in Fig. 1. Our approach based on fluid dynamics allows us to accurately model the initial concentration around the sensor by taking into account the droplet-air interaction and the narrowing beamwidth.

If the spatial distribution of droplets is assumed to be homogeneous, the mass of droplets in the inner cone can be found via multiplying the total transmitted mass, i.e., m_{TX}, by the ratio of the cone volumes, i.e., V_{rc}/V_c. However, due to the interactions among droplets and air molecules, the propagation of droplets is far from homogeneity [16]. Therefore, in order to quantify the inhomogeneous propagation of droplets, we define the spray coefficient (γ). By employing the ratio of the volumes, i.e., V_{rc}/V_c, and γ, a scaling factor (η) can be introduced to obtain the mass of droplets in V_{rc} as given by

$$\eta = \frac{V_{rc}}{V_c}\gamma = \frac{\frac{\pi}{3}s(s\tan\theta_{rv})^2}{\frac{\pi}{3}s(s\tan\theta)^2}\gamma = \left(\frac{\tan\theta_{rv}}{\tan\theta}\right)^2\gamma, \quad (1)$$

where $1 \leq \gamma \leq V_c/V_{rc}$. Here, $\gamma = 1$ means that the spatial distribution of droplets are homogeneous within the beamwidth of the outer cone (2θ), and $\gamma = V_c/V_{rc}$ means that all droplets propagate in the beamwidth of the inner cone ($2\theta_{rv}$). Then, the initial droplet concentration in the beamwidth of the RV (C_0) is derived by employing (1) as follows:

$$C_0 = \frac{m_{TX}\eta}{V_c} = \frac{m_{TX}\left(\frac{\tan\theta_{rv}}{\tan\theta}\right)^2\gamma}{\frac{\pi}{3}s\left(\frac{R_{rv}}{2}\right)^2} = \frac{3m_{TX}\gamma}{\pi s^3(\tan\theta)^2}. \quad (2)$$

Here, C_0 is assumed as the initial value of the time-dependent concentration in the RV ($C(t)$) which is derived in the next part of the paper. In (2), m_{TX} can be presented by using the volumetric flow rate (Q) of the TX which gives the fluid volume flowing through the sprayer per unit time [18]. Here, $Q = V_{TX}/T_e$ where V_{TX} shows the emitted liquid volume. Since the transmitted mass can be written as $m_{TX} = V_{TX}\rho_d$ where ρ_d is the density of the liquid forming droplets before

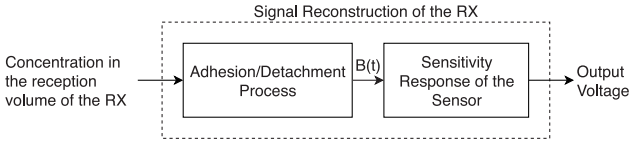

Fig. 3. Block Diagram of the Signal Reconstruction.

spraying, (2) is given by

$$C_0 = \frac{3QT_e\rho_d\gamma}{\pi s^3(\tan\theta)^2} = \frac{3V_{TX}\rho_d\gamma}{\pi(s\tan\theta)^2 s}. \tag{3}$$

In fluid dynamics, the effects of some parameters such as the length or volume can be reduced by using dimensionless parameters. These dimensionless parameters are also utilized for a more concise expression [18]. To this end, the characteristic length (L_c) is defined as

$$L_c = \frac{V_{TX}}{A_c} = \frac{V_{TX}}{\pi(s\tan\theta)^2} \tag{4}$$

where A_c is the cross-sectional area of the outer cone. By using L_c, a dimensionless parameter (s^*) as the normalized distance is defined as $s^* = s/L_c$. Hence, (3) is simplified as given by

$$C_0 = \frac{3\rho_d\gamma}{s^*}. \tag{5}$$

2) Signal Reconstruction of the Receiver: For our scenario, the reconstruction of the molecular signal around the RX is subject to an error due to the random adhesions/detachments of droplets to/from the sensor and the sensitivity of the sensor. Hence, the SR is modeled as the combination of the adhesion/detachment process and the sensitivity response of the sensor as shown in Fig. 3.

Let *X* and *Y* represent the droplets in the RV and the adhered droplet-sensor complex, respectively. Moreover, *Z* is defined as the detached state of the droplet which is assumed not to be sensed by the sensor. In order to provide a better understanding, an analogy between the adhesion/detachment process of droplets and the reception process of a biological cell which captures/releases molecules with its receptors can be established. Here, droplets are assumed to arrive the RV instantaneously after the emission in order to relate the chemical kinetics of droplets in the RV and the sensor measurement as a function of time. The adhesion and detachment can be modeled as first order reactions which are given by

$$\mathrm{X} \xrightarrow{\mathrm{k_1}} \mathrm{Y} \xrightarrow{\mathrm{k_2}} \mathrm{Z}, \tag{6}$$

where k_1 and k_2 are the rate constants of the corresponding reaction. Let $C(t)$ and $B(t)$ denote the concentrations of *X* and *Y* in kg/m^3, respectively. Based on the reaction system in (6) and the rate law [19], the concentrations $C(t)$ and $B(t)$ can be characterized as

$$\frac{dC(t)}{dt} = -k_1 C(t) \tag{7}$$

$$\frac{dB(t)}{dt} = k_1 C(t) - k_2 B(t), \tag{8}$$

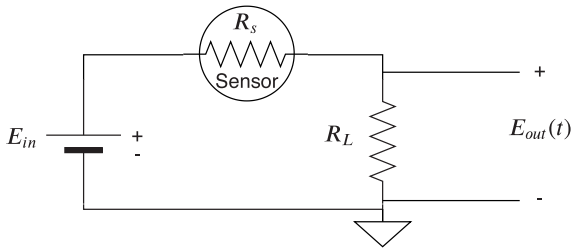

Fig. 4. Sensor Measurement Circuit.

where the initial conditions are defined as $C(0) = C_0$ and $B(0) = 0$. The solution of (7)-(8) for $B(t)$ can be given as

$$B(t) = \frac{k_1 C_0}{k_2 - k_1}\left[e^{-k_1 t} - e^{-k_2 t}\right]. \tag{9}$$

Subsequent to adhesion/detachment process, $B(t)$ is converted to an electrical signal by the metal-oxide MQ-3 sensor. Sensors of this type measure the concentration around them by changing their resistance so that each concentration value corresponds to a sensor resistance (R_s) value as shown in Fig. 4. In order to normalize the measured R_s, R_o is defined as the sensor resistance measured at 0.0004 kg/m^3 [20]. For each concentration value, R_s/R_o determines how sensitive the sensor can measure. This sensitivity characteristic, whose values are taken from its datasheet [20], can be employed to obtain a sensitivity function ($f(t)$) which maps concentration values to R_s/R_o values via curve fitting technique. The datasheet values are fitted by using nonlinear least squares method which minimizes the sum of square errors. $f(t)$ can be fitted as given by

$$f(B(t)) = 0.0116(B(t))^{-0.5855} - 0.0743 = \frac{R_s}{R_o}, \tag{10}$$

where $B(t)$ is the input to the sensitivity response of the sensor as shown in Fig. 3 and derived in (9). The scalar curve fitting parameters are estimated by employing Levenberg-Marquardt algorithm which has an estimation performance with the Root Mean Square Error (RMSE) value of 0.0371 [21].

In our experimental setup, the sensor measurement is made with a circuit as given in Fig. 4 where R_L is the load resistance, E_{in} is the input voltage and $E_{out}(t)$ is the output voltage which also gives the end-to-end system impulse response for an impulsive input signal. Using this circuit, R_s can be derived via Kirchhoff's voltage law [22] as given by

$$R_s = \left(\frac{E_{in}}{E_{out}(t)} - 1\right)R_L, \tag{11}$$

where E_{in} is given as 5 V in [20]. By combining (10) and (11), the relation between $f(B(t))$ and the parameters of the sensor measurement circuit can be written as

$$f(B(t)) = \left(\frac{E_{in}}{E_{out}(t)} - 1\right)\frac{R_L}{R_o}. \tag{12}$$

By using (12), $E_{out}(t)$ is given as

$$E_{out}(t) = \frac{E_{in}R_L}{R_o\left(f(B(t)) + \frac{R_L}{R_o}\right)}. \tag{13}$$

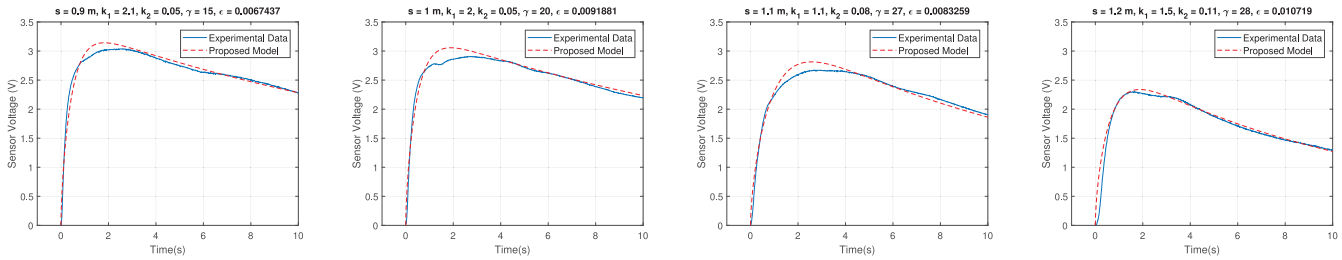

Fig. 5. The comparisons of the proposed model with experimental data for the parameters given in the title of each signal.

Finally, the end-to-end impulse response can be expressed by substituting (9) into (13) as given by

$$E_{out}(t) = \frac{E_{in} R_L}{R_o \left[f\left(\frac{k_1 C_0}{k_2 - k_1} \left(e^{-k_1 t} - e^{-k_2 t} \right) \right) + \frac{R_L}{R_o} \right]}, \qquad (14)$$

where it is important to note that C_0 is a function of the spray coefficient γ as given in (3). Therefore, the impulse response in (14) involves three novel channel parameters, i.e., k_1, k_2 and γ. These parameters are affected by the change of other parameters in the channel such as the distance between the TX and RX. Especially, γ depends on the type of the sprayer's nozzle which affects the spraying pattern [23] and interactions among droplets and air molecules. For numerical results, k_1, k_2, and γ are manually configured by making the Mean Square Error (ϵ) between the samples of $E_{out}(t)$ and experimental signal ($F(t)$) as small as possible according to the formula which is given as

$$\epsilon = \frac{1}{N} \sum_{n=1}^{N} (E_{out}[n] - F[n])^2 \qquad (15)$$

where N shows the number of samples, $E_{out}[n]$ and $F[n]$ are discrete-time representations of $E_{out}(t)$ and $F(t)$, respectively. Next, it is shown by numerical results that the proposed model given in (14) can be used for practical scenarios.

III. Numerical Results

A. Measurements

In order to measure Q, the sprayer is placed on a precision balance. For each measurement, the liquid is sprayed from the sprayer for a short interval (Δt_v). The mass of the sprayer is measured before and after spraying. Hence, the mass difference is found by measuring the mass values before and after spraying. By dividing the mass difference to ρ_d, the volume difference (ΔV) is calculated for each measurement. Thus, Q can be presented by [18]

$$Q = \frac{\Delta V}{\Delta t_v}. \qquad (16)$$

Here, the average of ten measurements is considered for Q. In addition, R_o is calculated by using $E_{out}(t)$ value when the concentration value is 0.0004 kg/m^3. The detection scope of the sensor which is between 5×10^{-5} and 10^{-2} kg/m^3, is scaled for $E_{out}(t)$ values between 0 and 5 V [20]. Hence, $E_{out}(t) = 0.2$ V for the concentration value of 0.0004 kg/m^3.

TABLE I
Experimental Parameters

Parameter	Value
Distance between the TX and RX (s)	$\{0.9, 1, 1.1, 1.2\}$ m
Volumetric flow rate (Q)	2.204×10^{-6} m^3/s
Density of liquid ethanol (ρ_d)	789 kg/m^3
Emission time of the TX (T_e)	0.5 s
Load resistance (R_L)	1 kΩ
Sensor resistance at 0.0004 kg/m^3 (R_o)	24 kΩ
Half-beamwidth of the sprayer (θ)	38°

Then, R_o is calculated by (11). Furthermore, θ is measured with ImageJ software using the image given in Fig. 1. Next, the values of the experimental parameters given in Table I are used for the validation of the proposed model.

B. Results for Channel Modeling

In Fig. 5, the comparisons of experimental data and the proposed model are shown. For performance evaluation, ϵ is calculated for a duration of 10 s. Fig. 5 validates that the proposed channel model can be employed to estimate the received signal.

As proposed in [24] for diffusion-based MC in microscale, the SR of the RX may result in error due to the random movements of the molecules in the reception volume. Accordingly for our macroscale scenario, k_1 and k_2 represent the average characteristic of the random movements of the droplets in the RV. In addition, γ describes the effect of the two-phase flow on the initial concentration in the RV. As shown in Fig. 5, γ increases as s increases, since the shape of droplets' spatial dispersion gets narrower with s. The increment of γ with s validates the narrowing beamwidth at longer distances due to the droplet-air interaction [16]. Moreover, the slope of the rising edge of the signals in Fig. 5 between 0 and peak time is proportional to k_1. This slope decreases as s increases, since k_1 is proportional to the energy of droplets entering the RV. At longer distances, the droplet-sensor interaction in the RV decreases due to the decreasing droplet energy. In addition, as k_2 increases, the adhered droplets on the sensor detach faster and the sensor voltage drops faster from its peak value to its initial level.

In Fig. 6, twenty different manually fitted signals (with a ϵ of less than 0.021) are used to observe the relation of k_1 and k_2 with the normalized distance (s^*). Droplets are more unlikely to stay adhered to the sensor due to the decreasing energy of droplets for longer distances, as shown with the change of

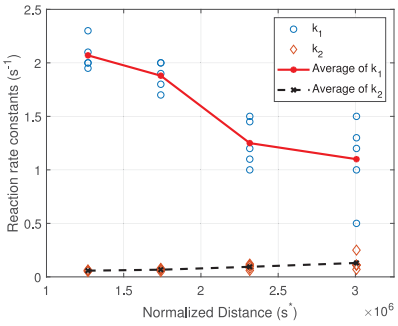

Fig. 6. The relation of k_1 and k_2 with the normalized distance.

average k_1 values in Fig. 6. In contrast to k_1, k_2 is almost constant, since the energy of droplets is not so effective on their detachment from the sensor in the RV. Although physically measurable parameters (k_1, k_2, γ) are proposed for the channel model, there is a need for further research effort to investigate the relation of these parameters with the environmental conditions.

IV. Conclusion

In this article, an end-to-end system model is proposed for macroscale sprayer-based MC systems. Our model takes the liquid droplets as information carriers into account with a signal reconstruction approach. The signal reconstruction of the RX considers the adhesion/detachment of droplets and the sensor's sensitivity. This study reveals the physical meanings of the channel parameters for sprayer-based MC systems. Furthermore, it is essential to highlight that these practical MC systems can be implemented for the research in airborne pathogen transmission with a MC perspective. In a communication system where the TX is a person emitting pathogen-laden droplets via sneezing/coughing and the RX is a biological sensor, our proposed end-to-end system model can be applied for the detection of pathogens. As the future work, we plan to employ our proposed approach for channel parameter estimation and investigate what the proposed novel channel parameters depend on.

References

[1] N. Farsad, W. Guo, and A. W. Eckford, "Tabletop molecular communication: Text messages through chemical signals," *PLoS ONE*, vol. 8, no. 12, 2013, Art. no. e82935.

[2] B.-H. Koo, C. Lee, H. B. Yilmaz, N. Farsad, A. Eckford, and C.-B. Chae, "Molecular MIMO: From theory to prototype," *IEEE J. Sel. Areas Commun.*, vol. 34, no. 3, pp. 600–614, Mar. 2016.

[3] N. Farsad, D. Pan, and A. Goldsmith, "A novel experimental platform for in-vessel multi-chemical molecular communications," in *Proc. IEEE Global Commun. Conf. (GLOBECOM)*, pp. 1–6.

[4] L. Khaloopour *et al.*, "An experimental platform for macro-scale fluidic medium molecular communication," *IEEE Trans. Mol. Biol. Multi-Scale Commun.*, vol. 5, no. 3, pp. 163–175, Dec. 2019.

[5] H. Unterweger *et al.*, "Experimental molecular communication testbed based on magnetic nanoparticles in duct flow," in *Proc. IEEE 19th SPAWC*, 2018, pp. 1–5.

[6] D. T. McGuiness, S. Giannoukos, A. Marshall, and S. Taylor, "Parameter analysis in macro-scale molecular communications using advection-diffusion," *IEEE Access*, vol. 6, pp. 46706–46717, 2018.

[7] M. Abbaszadeh *et al.*, "Mutual information and noise distributions of molecular signals using laser induced fluorescence," in *Proc. IEEE Global Commun. Conf.*, 2019, pp. 1–6.

[8] S. Qiu *et al.*, "Long range and long duration underwater localization using molecular messaging," *IEEE Trans. Mol. Biol. Multi-Scale Commun.*, vol. 1, no. 4, pp. 363–370, Dec. 2015.

[9] F. Gulec and B. Atakan, "Localization of a passive molecular transmitter with a sensor network," in *Proc. Int. Conf. Bio-Inspired Inf. Commun.*, 2020, pp. 317–335.

[10] F. Gulec and B. Atakan, "Distance estimation methods for a practical macroscale molecular communication system," *Nano Commun. Netw.*, vol. 24, May 2020, Art. no. 100300.

[11] M. Khalid, O. Amin, S. Ahmed, B. Shihada, and M.-S. Alouini, "Communication through breath: Aerosol transmission," *IEEE Commun. Mag.*, vol. 57, no. 2, pp. 33–39, Feb. 2019.

[12] N. Farsad, N.-R. Kim, A. W. Eckford, and C.-B. Chae, "Channel and noise models for nonlinear molecular communication systems," *IEEE J. Sel. Areas Commun.*, vol. 32, no. 12, pp. 2392–2401, Dec. 2014.

[13] N.-R. Kim, N. Farsad, C.-B. Chae, and A. W. Eckford, "A universal channel model for molecular communication systems with metal-oxide detectors," in *Proc. IEEE Int. Conf. Commun. (ICC)*, pp. 1054–1059.

[14] M. Abbaszadeh, P. J. Thomas, and W. Guo, "Toward high capacity molecular communications using sequential vortex rings," *IEEE Trans. Mol. Biol. Multi-Scale Commun.*, vol. 4, no. 1, pp. 39–42, Mar. 2018.

[15] J. Li, W. Zhang, X. Bao, M. Abbaszadeh, and W. Guo, "Inference in turbulent molecular information channels using support vector machine," *IEEE Trans. Mol. Biol. Multi-Scale Commun.*, vol. 6, no. 1, pp. 25–35, Jul. 2020.

[16] S. Ghosh and J. C. R. Hunt, "Induced air velocity within droplet driven sprays," *Proc. R. Soc. A*, vol. 444, no. 1920, pp. 105–127, 1994.

[17] M. Ishii and T. Hibiki, *Thermo-Fluid Dynamics of Two-Phase Flow*. New York, NY, USA: Springer, 2010.

[18] B. R. Munson, D. F. Young, T. H. Okiishi, and W. W. Huebsch, *Fundamentals of Fluid Mechanics*. Hoboken, NJ, USA: Wiley, Inc., 2009.

[19] P. Atkins and J. De Paula, *Physical Chemistry*. New York, NY, USA: Freeman, 2010.

[20] *Technical Data of MQ-3 Gas Sensor*, Hanwei-Electron. Group Corp., Henan, China, 2018.

[21] M. T. Hagan and M. B. Menhaj, "Training feedforward networks with the Marquardt algorithm," *IEEE Trans. Neural Netw.*, vol. 5, no. 6, pp. 989–993, Nov. 1994.

[22] J. W. Nilsson and S. Riedel, *Electric Circuits*. Upper Saddle River, NJ, USA: Prentice Hall Press, 2010.

[23] M. Al Heidary, J. P. Douzals, C. Sinfort, and A. Vallet, "Influence of spray characteristics on potential spray drift of field crop sprayers: A literature review," *Crop Prot.*, vol. 63, pp. 120–130, Sep. 2014.

[24] B. Atakan and F. Gulec, "Signal reconstruction in diffusion-based molecular communication," *Trans. Emerg. Telecommun. Technol.*, vol. 30, no. 12, 2019, Art. no. e3699.